MondoScience
Est 2016

Modern Materials: Hyperelastic Materials and Advanced Elastomer Systems

Continuing Education for Professional Engineers

PREPARED BY :
MondoScience

CONTACT :
Online-PDH, Cadistics, LLC
www.online-pdh.com
Email: cadistics@yahoo.com

Course description

Hyperelastic and advanced elastomer materials are critical in seals, mounts, biomedical devices, and soft robotic systems. Their unique ability to undergo large, reversible deformations requires specialized modeling and design approaches.

This course introduces the fundamentals of hyperelasticity, key constitutive models, testing methods, and material families. It also covers durability, environmental effects, and the use of finite element analysis (FEA) for practical applications.

Learning objectives

Upon completion of this course, participants will be able to:

- Understand the principles of hyperelasticity and strain energy functions.
- Apply and compare common hyperelastic models such as Neo-Hookean, Mooney–Rivlin, Ogden, and Gent.
- Interpret test data and calibrate material models.
- Assess elastomer families for performance, durability, and compatibility.
- Implement hyperelastic models in FEA and validate against experimental data.

Intended audience

This course is designed for professional engineers working in disciplines such as mechanical, civil, biomedical, chemical, aerospace, and automotive engineering. It is particularly valuable for those involved in the design, analysis, or specification of elastomeric components, as well as engineers who rely on simulation tools to predict performance in demanding environments.

Table of Contents

Chapter 1: Fundamentals of Hyperelasticity: Kinematics, Thermodynamics, and Stress Measures

Context and Scope

Elastomers and elastomeric systems enable large, recoverable strains, complex nonlinear responses, and unusual combinations of stiffness, damping, and durability. Modeling them as **hyperelastic** materials means representing the Cauchy stress as fully determined by a strain-energy density function W and the current deformation.

This chapter establishes the kinematics at large strain, introduces the thermodynamic foundations of W, clarifies incompressibility and compressibility in rubber, and connects W to the stress measures commonly used in design and simulation. Foundational references include Ogden's monograph on finite elasticity and the classic Rivlin–Mooney papers that recast rubber elasticity in terms of invariants (Ogden, 1997; Mooney, 1940; Rivlin, 1948).

Large-Strain Kinematics

At large strain, the deformation gradient $\mathbf{F} = \delta / \delta \mathbf{X}$ maps material coordinates $\mathbf{X}$ to spatial coordinates $\mathbf{x}$. The right Cauchy–Green tensor is $\mathbf{C} = \mathbf{F}^T\mathbf{F}$; its invariants for isotropic materials are:

$$I_1 = \mathrm{tr}\mathbf{C}, \qquad I_2 = \tfrac{1}{2}\left[(\mathrm{tr}\mathbf{C})^2 - \mathrm{tr}(\mathbf{C}^2)\right], \qquad I_3 = \det \mathbf{C} = J^2$$

with $J = \det \mathbf{F}$ the local volume ratio.

For principal stretches

$$\lambda_1, \lambda_2, \lambda_3,\ I_1 = \lambda_1^2 + \lambda_2^2 + \lambda_3^2,\ I_2 = \lambda_1^2\lambda_2^2 + \lambda_2^2\lambda_3^2 + \lambda_3^2\lambda_1^2,\ I_3 = (\lambda_1\lambda_2\lambda_3)^2$$

These invariants underpin many hyperelastic models because they preserve frame indifference and isotropy (Ogden, 1997; Rivlin, 1948).

Formula keys.

$\mathbf{F}$ = deformation gradient

$\mathbf{C}$ = right Cauchy–Green tensor

I_1, I_2, I_3 = first, second, third invariants

λ_i = principal stretches
J = volume ratio.

Thermodynamic Statement: Strain-Energy and Stress

Under isothermal conditions, the constitutive response derives from a stored-energy density $W(\mathbf{C})$. For compressible materials,

$$\mathbf{S} = 2\frac{\delta W}{\delta \mathbf{C}}, \quad \sigma = \frac{1}{J}\,\mathbf{F}\,\mathbf{S}\,\mathbf{F}^T$$

where $\mathbf{S}$ is the second Piola–Kirchhoff stress and $\boldsymbol{\sigma}$ the Cauchy stress. For (nearly) incompressible rubber, it is standard to split:

$$W = \overline{W}(\overline{\mathbf{C}}) + U(J) \text{ with } \overline{\mathbf{C}} = J^{-2/3}\mathbf{C} \text{ (isochoric)}$$

and $U(J)$ the volumetric penalty; equivalently, enforce $J = 1$ by a Lagrange multiplier p (hydrostatic pressure),

$$\sigma = -p\mathbf{I} + \frac{2}{J}\,\mathbf{F}\,\frac{\delta \overline{W}}{\delta \mathbf{C}}\,\mathbf{F}^T$$

Hybrid/mixed finite elements are used in practice to avoid volumetric locking when $J \approx 1$ (Abaqus/ANSYS guidance).

Formula keys.

W = strain-energy density
$\mathbf{S}$ = 2nd Piola–Kirchhoff stress
$\boldsymbol{\sigma}$ = Cauchy stress
$\overline{W}$ = isochoric energy
$U(J)$ = volumetric energy
p = pressure (Lagrange multiplier)
$\mathbf{I}$ = identity tensor.

Stress Measures and What Engineers Actually Use

Designers move among nominal/engineering stress, true stress, and invariant-based stress. The choice affects parameter identification and safety factors.

Note that losing track of which measure a model or test reports is a frequent source of 10–30% fitting error in rubbers.

Table 1: The main stress measures at large strain.

Measure	Definition	Typical use	Notes
First Piola–Kirchhoff $\mathbf{P}$	$\mathbf{P} = \mathbf{FS}$	Relates forces to reference area	Not symmetric
Second Piola–Kirchhoff $\mathbf{S}$	$2\delta W / \delta \mathbf{C}$	Thermodynamics; model derivation	Symmetric in reference frame
Cauchy $\boldsymbol{\sigma}$	$^1/_J\ \mathbf{FSF}^T$	Physical (true) stress	Symmetric; acts on current area
Nominal stress P_{11} in uniaxial	Force/initial area	Material testing, ASTM/ISO	Convert carefully to σ

The invariant route yields $\boldsymbol{\sigma}$ once W is specified; testing typically reports nominal stress, so conversion must be consistent with kinematics (Ogden, 1997).

Incompressibility and bulk response of elastomers

Unfilled elastomers are highly incompressible: $\nu \to 0.499$ is common, implying $K / G \gg 10^2$. In simulations this calls for mixed u-p (hybrid) elements (e.g., C3D8H in Abaqus) or mixed formulations in ANSYS to avoid locking and spurious pressure (Abaqus, ANSYS). For slightly compressible fits one introduces a bulk term

$$U(J) = \frac{K}{2}(J-1)^2$$

or code-specific parameterizations (e.g., compressibility parameter d in ANSYS).

Formula keys.

υ = Poisson's ratio

K = bulk modulus

G = shear modulus

$u - p$ = mixed displacement–pressure formulation
d = compressibility parameter (solver-specific).

A first uniaxial specialization

For incompressible uniaxial extension with stretch λ, the lateral stretches satisfy $\lambda_2 = \lambda_3 = \lambda^{-1/2}$ so $J = \lambda\,\lambda^{-1/2}\,\lambda^{-1/2} = 1$. Given $W(\lambda)$, the nominal axial stress is

$$P = \frac{\delta W}{\delta \lambda}, \qquad \sigma = \lambda P$$

This identity underlies data-to-model fitting from ASTM D412/ISO 37 tensile tests (ASTM D412; ISO 37).

Formula keys.
λ = axial stretch
P = nominal stress
σ = true (Cauchy) stress.

Conclusion

Hyperelasticity rests on a compact thermodynamics: a scalar W captures all elastic responses at large strain. Choosing and calibrating W demands careful kinematics, awareness of stress measures, and an explicit strategy for (near) incompressibility that matches the FE element formulation.

Chapter 2: Constitutive Modeling: From Neo-Hookean to Ogden, Arruda–Boyce, and Gent

Why so Many Models?

Rubbers span carbon-black–filled NR, peroxide-cured EPDM, silicone LSRs, TPUs, and more. Their macromolecular physics (network density, finite chain extensibility, entanglements, filler networking) makes a single universal W unrealistic. Different models emphasize different physics or fitting convenience. We survey the most used families and state how to interpret parameters for engineering decisions (Mooney, 1940; Rivlin, 1948; Ogden, 1997; Arruda and Boyce, 1993; Gent, 1996).

Neo-Hookean and Mooney–Rivlin

The incompressible neo-Hookean model uses the first invariant:

$$W = \frac{\mu}{2}(I_1 - 3)$$

Mooney–Rivlin extends this to

$$W = \mathbf{C}_{10}(I_1 - 3) + \mathbf{C}_{01}(I_2 - 3)$$

with small-strain shear modulus $G = 2(\mathbf{C}_{10} + \mathbf{C}_{01})$. These models fit moderate strains (<100% –150%) and are often favored for simplicity, but may deviate at high stretch or in planar/biaxial states (Mooney, 1940; Rivlin, 1948; Ogden, 1997).

Formula keys.

μ = shear modulus

$\mathbf{C}_{10}$, $\mathbf{C}_{01}$ = Mooney–Rivlin parameters

G = small-strain shear modulus.

Yeoh and Ogden: curvature control and flexibility

The Yeoh model targets I1-driven curvature with higher-order terms:

$$W = \sum_{i=1}^{3} \mathbf{C}_{i0}(I_1 - 3)^i$$

The Ogden form uses principal stretches:

$$W = \sum_{i=1}^{N} \frac{\mu_i}{\alpha_i}(\lambda_1^{\alpha i} + \lambda_2^{\alpha i} + \lambda_3^{\alpha i} - 3)$$

giving excellent flexibility to match tension, compression, and biaxial data across large strains when $N \geq 2$ (Ogden, 1997).

Formula keys.

$\mathbf{C}_{i0}$ = Yeoh constants

μ_i, α_i = Ogden constants

λ_i = principal stretches.

Finite chain extensibility: Arruda–Boyce and Gent

Hyperelastic responses stiffen markedly as chains approach their contour length. Two well-established models capture this **strain hardening**:

Arruda–Boyce (eight-chain model).

$$W = \mu \sum_{n=1}^{5} \frac{\mathbf{C}_n}{\lambda_L^{2n-2}} (I_1 - 3)^n$$

where λ_L is the limiting network stretch (related to the number of Kuhn segments), $\mathbf{C}_n$ are known series coefficients, and μ the small-strain shear modulus (Arruda and Boyce, 1993).

Gent model.

$$W = -\frac{\mu J_m}{2} \ln\left(1 - \frac{\bar{I}_1 - 3}{J_m}\right)$$

with J_m a stiffening parameter proportional to the square of the limiting stretch; as $\bar{I}_1 \to 3 + J_m$ the stiffness diverges, reproducing the observed hardening (Gent, 1996).

Engineering takeaway. Arruda–Boyce gives a direct physics link to finite extensibility; Gent delivers a minimal two-parameter form with realistic asymptotes. Both are robust in high-stretch seals, balloons, and soft-robotic membranes where classic Mooney–Rivlin under-predicts (Arruda and Boyce, 1993; Gent, 1996).

Formula keys.

$\bar{I}_1$ = isochoric first invariant
λ_L = limiting stretch
$\mathbf{C}_n$ = series coefficients
J_m = Gent stiffening parameter.

Filled elastomers: Payne and Mullins phenomena

Carbon black or silica reinforcement raises stiffness, introduces amplitude-dependent moduli (Payne effect), and causes stress-softening after first loading (Mullins effect). These require either pseudoelastic softening terms or coupling to viscoelasticity. Reviews and models include Bergström–Boyce for rate-dependence and Mullins-type internal variables (Bergström & Boyce, 1999; Diani et al., 2009; Qi & Boyce, 2004).

Engineering takeaway. If your test program includes cyclic amplitude sweeps or first-cycle vs stabilized loops, a purely elastic W will not suffice; add softening/viscoelastic terms or use coupled hyper-viscoelastic models (Bergström & Boyce, 1999).

Model selection in practice

Start from intended strain range and loading modes (uniaxial, planar, biaxial), then decide:

- Low–moderate strain seals/grommets: two-parameter Mooney–Rivlin or Yeoh (I1).
- High-stretch membranes, balloons, soft actuators: Ogden $N \geq 2$, Arruda–Boyce, or Gent.
- Filled, rate-dependent bushings/mounts: hyper-viscoelastic with Mullins/Payne augmentations.

In all cases, match FE formulation to compressibility assumption (hybrid $u - p$ for near-incompressible) (Abaqus/ANSYS).

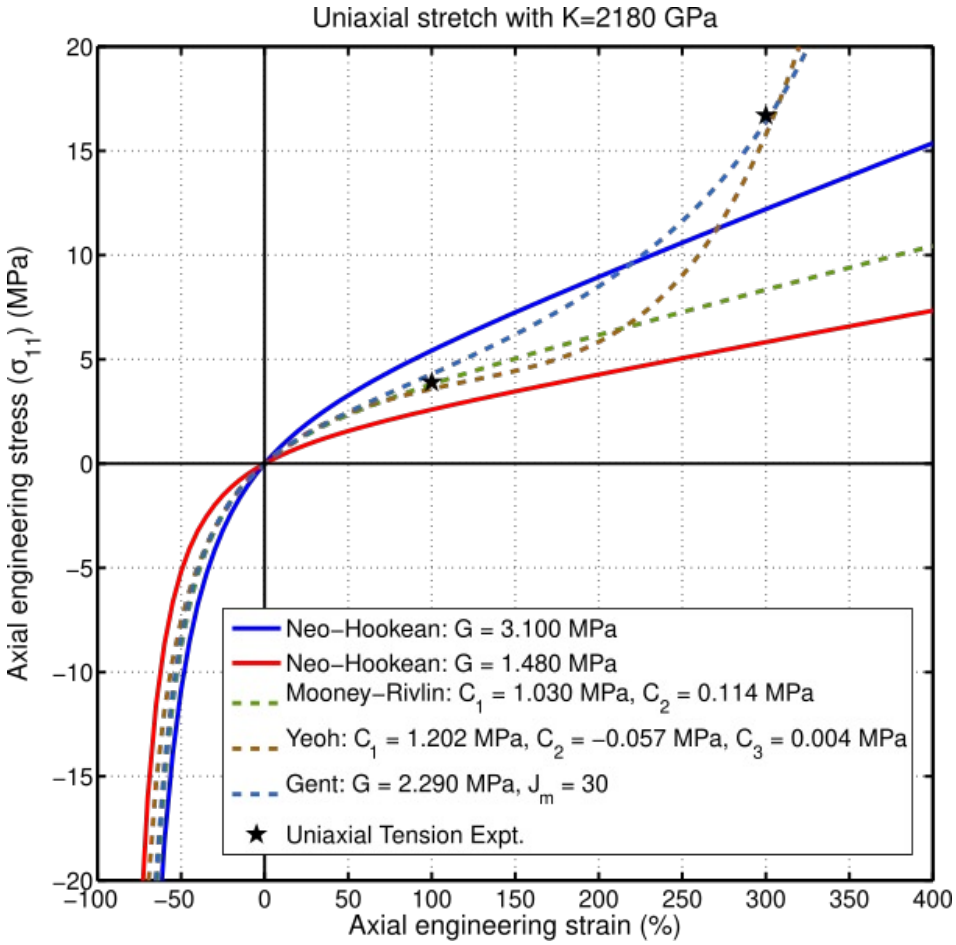

Figure 1: stress–stretch curves comparing Mooney–Rivlin, Yeoh, Ogden-2, Gent for a high-stretch silicone

Credit: Bbanerje, via Wikimedia Commons

Figure 1 shows how finite-extensibility models capture the sharp upturn beyond $\lambda \approx 2$, while two-term MR tends to under-predict.

Conclusion

No single model is “best.” Select the minimal form that reproduces the required states of strain and rate effects with parameters that your test program can reliably identify. Where finite extensibility or filler networking matter, Gent/Arruda–Boyce or augmented hyper-viscoelastic formulations are superior to classical two-term MR.

Chapter 3: Characterization and Data Reduction: From the Lab Bench to Reliable Model Fits

Overview

The quality of any hyperelastic simulation rests on the testing and data reduction. Here we outline tensile, planar, and biaxial protocols; hardness and compression set as screening metrics; dynamic mechanical analysis for viscoelasticity; and cure rheometry for compounding. Referencing the relevant international standards is needed so test plans are auditable and traceable (ASTM D412; ISO 37; ASTM D2240; ISO 815-1; ISO 4666).

Quasi-Static Mechanical Tests for Hyperelastic Fitting

Tensile stress–strain per ASTM D412 or ISO 37 provides nominal stress vs stretch from dumbbell specimens. Planar (strip) and biaxial (inflation or cruciform) tests are recommended when fitting multi-parameter models to avoid non-uniqueness. Always record width/thickness evolution if converting to Cauchy stress (ASTM D412; ISO 37). These standards enable consistent inter-lab comparisons and ensure your FE material card reflects physical reality

Table 2 links each standard to its primary modeling use (ASTM D412; ISO 37; ASTM D2240; ASTM D395; ISO 815-1; ISO 4666).

Table 2: Common standards for rubber characterization (selected).

Property	Standard	What it gives	Typical role in modeling
Tension	ASTM D412 / ISO 37	Nominal stress–strain, ultimate	Base data for W fit
Hardness	ASTM D2240	Shore A/D indentation	Quick QC correlation to G
Compression set	ASTM D395 / ISO 815-1	Permanent set after compression	Seal longevity proxy
Dynamic fatigue/ temperature rise	ISO 4666	Flexometer fatigue & heat build-up	Durability & hysteresis

DMA and WLF: Rate/Temperature Mapping

Dynamic Mechanical Analysis (DMA) measures storage E' and loss E'' vs frequency/temperature. Time–temperature superposition builds master curves and, above T_g, the shift factor often follows the Williams–Landel–Ferry (WLF) equation:

$$\text{Log}_{10}\, a_T = -\frac{C_1(T - T_r)}{C_2 + (T - T_r)}$$

WLF parameters (C_1, C_2) are fit from DMA and used to scale viscoelastic spectra into simulation or to define temperature-dependent damping (Williams, Landel and Ferry, 1955; Ferry, 1980).

Formula keys.

a_T = horizontal shift factor
T = test temperature
T_r = reference temperature
C_1, C_2 = WLF constants
E', E'' = storage/loss moduli.

Cure Rheometry and Process Control

Moving-Die Rheometer (MDR) or Rotorless Cure Meter per ASTM D5289 quantifies scorch time, cure rate, and plateau torque. These inform crosslink density targets and data scatter in W fits, especially for peroxide-cured EPDM and silicone where post-cure matters (ASTM D5289 guides).

Data Reduction: From Raw Curves to Model Coefficients

A consistent pipeline looks like this:

(i) convert force–displacement to nominal stress–stretch with careful geometry tracking;
(ii) choose stress measure consistent with your W derivation;
(iii) perform multi-mode fitting (tension + planar + biaxial) to constrain parameters;
(iv) validate on independent load cases (compression, shear).

Most FE solvers support direct fitting from test data to hyperelastic coefficients and recommend hybrid elements for near-incompressible rubber (Abaqus documentation).

Special Issues with Filled Rubbers

Amplitudes matter: small-strain dynamic sweeps display the Payne effect (modulus decreases with strain amplitude); first-cycle softening and hysteresis reflect Mullins and viscoelasticity. If design loads are cyclic, include amplitude-dependent tests and fit parameters for softening models or coupled viscoelasticity (Bergström & Boyce, 1999; Diani et al., 2009).

Safety, Durability, and Fracture Data

For fatigue and tearing, the Lake–Thomas framework relates crack growth to a tearing energy T; pure-shear tests per Rivlin–Thomas yield T values relevant to cut-growth and endurance limits (Lake and Thomas, 1967; Rivlin and Thomas, 1953; Elmukashfi et al., 2021). Incorporating T into design allows screening of compounds for crack-growth resistance in flex-fatigue (e.g., mounts, tires).

Conclusion

Sound models come from sound data. Use multiple deformation modes, keep the stress measure consistent, include rate/temperature mapping when needed, and, crucially, reflect filler-induced softening in your test plan if the application will experience cyclic or amplitude-dependent loads. Standards-anchored testing and disciplined data reduction produce material cards that generalize beyond the lab (ASTM/ISO; Ferry, 1980).

Chapter 4: Advanced Elastomer Systems: Families, Chemistry, and Selection

Introduction

Hyperelastic modeling is only as useful as the knowledge of the materials themselves. Elastomers vary widely in backbone chemistry, curing methods, filler systems, and resulting property windows. This chapter surveys the main elastomer families, drawing links between their chemistry, structure, and engineering performance. Emphasis is placed on practical selection for chemical resistance, thermal range, dynamic fatigue, biocompatibility, and cost. Standard references include ASTM, ISO, and detailed monographs (Mark et al., 2013; Roland, 2011).

Natural and synthetic rubbers

- **Natural rubber (NR):** Derived from polyisoprene latex, NR is notable for high resilience, strain crystallization, and exceptional fatigue resistance (Lake and Thomas, 1967). However, NR has poor resistance to ozone and hydrocarbons, requiring antiozonants and compounding.
- **Styrene–butadiene rubber (SBR):** Copolymerized from styrene and butadiene, SBR has good abrasion resistance and cost-effectiveness, making it a dominant tire material. Its glass transition is higher than NR, reducing low-temperature flexibility (Ward and Sweeney, 2013).
- **Butadiene rubber (BR):** Offers excellent low-temperature flexibility, used in blends with SBR and NR.

Diene-based synthetic elastomers

- **Nitrile rubber (NBR):** Acrylonitrile content (18–50%) controls oil and fuel resistance but raises glass transition, sacrificing low-temperature properties.
- **Hydrogenated nitrile rubber (HNBR):** Hydrogenation removes double bonds, raising heat and ozone resistance, with good dynamic fatigue strength, making it suitable for automotive seals and timing belts (Bayer technical datasheets).
- **Ethylene–propylene–diene monomer (EPDM):** Offers outstanding weather, ozone, and water resistance. Its saturated backbone makes it chemically stable but poorly oil resistant. Widely used in automotive

weatherstrips, roofing membranes, and cable insulation (Mark et al., 2013).

High-performance fluorinated systems

- **Fluoroelastomers (FKM, FFKM):** Incorporating fluorine raises chemical inertness, low fuel permeability, and high-temperature performance (200–300 °C). FFKM offers nearly universal chemical resistance but is costly. Widely specified in aerospace, oil and gas, and semiconductor applications (Liu and Wu, 2012).
- **Silicone rubber (VMQ, FVMQ):** Siloxane backbone gives low glass transition (~−120 °C) and wide operating window (−60 to +200 °C), biocompatibility, and low toxicity. Poor tear and abrasion resistance are mitigated with fillers or blends (Roland, 2011).

Table illustrates property–application mapping across elastomer families.

Table 3: Summary of major elastomer families and their strengths/weaknesses.

Elastomer	Key strengths	Key weaknesses	Common uses
NR	Fatigue, resilience	Ozone, oil resistance	Tires, antivibration
SBR	Abrasion, cost	Low-T flexibility	Tires
NBR	Oil resistance	Low-T brittleness	Fuel hoses, seals
HNBR	Oil + ozone resistance	Cost	Automotive timing belts
EPDM	Weathering, water	Oil, fuels	Roofing, seals
FKM	Heat + chemicals	Cost	Aerospace seals
VMQ	Wide temp, biocompat.	Tear strength	Medical tubing

Thermoplastic elastomers (TPEs and TPVs)

Thermoplastic polyurethanes (TPU), thermoplastic vulcanizates (TPV), and thermoplastic copolyesters (TPEE) combine elastomeric flexibility with thermoplastic processability. Their advantages are recyclability and rapid processing; disadvantages include reduced high-temperature and fluid resistance compared to crosslinked rubbers (Holden et al., 2004).

Engineering selection strategies

Engineers typically screen elastomers via a compatibility matrix of temperature, fluids, and mechanical demands. For instance, FKM is selected for aerospace fuel seals; EPDM for potable water; VMQ for biomedical implants. Modern databases (ASTM D2000, SAE J200) provide grade coding for automotive elastomers (Ward and Sweeney, 2013).

Conclusion

The diversity of elastomer families allows targeted solutions, from low-cost SBR blends in tires to FFKM in semiconductor seals. Understanding backbone chemistry, cure systems, and fillers is essential to aligning elastomer performance with design requirements. A knowledge of both commodity and high-performance systems empowers engineers to select materials that balance cost, durability, and compliance.

Chapter 5: Durability, Fracture, and Environmental Effects

Introduction

While elastomers can endure large reversible strains, their durability depends on fatigue, crack growth, and environmental exposure. Engineers must assess long-term properties under cyclic load, ozone, UV, heat, fluids, and creep. This chapter discusses fracture mechanics of elastomers, the Mullins effect, tearing energy, and accelerated aging methodologies. Standard frameworks are drawn from Lake–Thomas tearing theory, ISO fatigue standards, and viscoelastic fracture literature (Lake and Thomas, 1967; Rivlin and Thomas, 1953; Mars and Fatemi, 2004).

Fracture mechanics of elastomers

Elastomers fail by crack growth rather than bulk yielding. The relevant parameter is *tearing energy* T, defined as the change in stored elastic energy per unit crack growth. In a pure shear specimen (Rivlin–Thomas geometry),

$$T = W\ 2h$$

where W is strain energy density and h the specimen half-height (Rivlin and Thomas, 1953).

Lake–Thomas theory relates T to chain scission at the crack tip, explaining why fatigue resistance correlates with network architecture (Lake and Thomas, 1967).

Formula keys.

T = tearing energy
W = strain energy density
h = half-height of specimen.

Fatigue and crack growth

Dynamic flex fatigue produces cumulative crack growth even at stresses well below ultimate. Crack growth rate $dc/\ dN$ often follows a Paris-type relation in terms of T. Mars and Fatemi (2004) provide detailed models linking strain energy

release to fatigue life. Carbon black reinforcement improves crack growth resistance via strain crystallization and filler toughening (Mars and Fatemi, 2004).

Environmental degradation

- **Ozone and UV:** Unsaturated rubbers (NR, SBR, NBR) undergo surface cracking unless protected by wax bloom or antiozonants (Crack et al., 2010).
- **Thermal aging:** Oxidation leads to chain scission or crosslinking, shifting modulus and embrittlement. Arrhenius time–temperature extrapolation is widely used to predict service life (Ferry, 1980).
- **Fluid swell:** Fickian diffusion of hydrocarbons increases volume and lowers modulus. Permeation is quantified by ASTM D471, important for fuel and chemical seals.

Viscoelastic creep and stress relaxation

Elastomers exhibit stress relaxation in compression and creep under sustained loads. For seals, stress relaxation translates into reduced contact force over years, driving leakage. These effects are modeled with Prony series fitted from DMA, then superposed with hyperelasticity in FE solvers (Roland, 2011).

Design approaches to durability

Engineers mitigate durability risks by:

- Selecting filled NR or HNBR for fatigue-critical applications.
- Using FKM for high-temperature chemical exposure.
- Designing seals with extra squeeze to offset relaxation.
- Performing accelerated aging (thermal/ozone chambers) and extrapolating to service conditions with Arrhenius/WLF models.

Conclusion

Elastomers rarely fail from one-off overload; they fail from fatigue, crack growth, or environment-driven degradation. Tearing energy, Mullins softening, ozone resistance, and stress relaxation must all be considered to ensure reliable service. By combining fracture mechanics, accelerated aging protocols, and material-specific knowledge, engineers can design elastomer systems that maintain sealing, damping, and structural performance over decades.

Chapter 6: Finite Element Implementation and Validation of Hyperelastic Models

Introduction

Finite element analysis (FEA) is the dominant engineering tool for applying hyperelastic material models to design. While the constitutive laws of Chapters 1–2 define the theory, their correct application in simulation requires careful numerical implementation. Issues of near-incompressibility, element choice, convergence, and validation are critical. Missteps can yield misleading stress fields or nonphysical results.

This chapter develops a detailed framework for implementation, calibration, and validation. References include Ogden (1997), ABAQUS and ANSYS documentation, and published guidelines on numerical stability (Belytschko et al., 2014; Holzapfel, 2000).

Near-Incompressibility and Hybrid Elements

Elastomers exhibit Poisson's ratios close to 0.5 ($\nu \approx 0.499$), meaning bulk modulus K is orders of magnitude greater than shear modulus G. Standard displacement-based elements cannot accommodate this without volumetric locking. Hybrid or mixed u-p formulations are recommended (e.g., C3D8H in ABAQUS, Plane182 with hybrid option in ANSYS). These allow pressure as an independent field variable, enforcing incompressibility without spurious stiffness (ABAQUS docs).

Formula key.

ν = Poisson's ratio
K = bulk modulus
G = shear modulus
u = displacement DOF
p = pressure DOF.

Element Formulations and Integration

Reduced integration (one-point Gauss) alleviates locking but risks hourglassing. Enhanced strain and selective reduced integration mitigate these issues. Hexahedral hybrid elements are generally superior for seals and mounts, while tetrahedral hybrids (C3D10H) serve complex geometries at greater computational cost (Belytschko et al., 2014).

Boundary Conditions, Loading, and Convergence

Hyperelastic materials stiffen at large strain, leading to nonlinear load–displacement curves and convergence difficulties. Incremental loading, automatic stabilization, and viscous damping are used to aid convergence. For seal analyses, large-deformation contact with friction introduces additional nonlinearities. Appropriate penalty or augmented Lagrange methods are recommended to ensure accurate stress transfer without artificial stiffness (Holzapfel, 2000).

Calibration Workflow

Calibration proceeds in four steps:

1. Convert test data (tensile, planar, biaxial) into stress–stretch curves.
2. Select candidate models (e.g., Mooney–Rivlin, Ogden).
3. Fit coefficients via nonlinear regression, using multi-mode data to avoid overfitting.
4. Validate predictions against independent load cases (compression, shear, inflation).

A good practice is to report 95% confidence intervals on fitted parameters and evaluate sensitivity of predictions to parameter perturbations (Mars and Fatemi, 2004).

Validation Strategies

Validation requires comparing FE-predicted force–displacement with test data not used in calibration. For example, fit to tensile/planar data, then validate against equi-biaxial inflation or indentation. Independent validation is critical for certification in aerospace or medical devices.

Table 4 illustrates that calibration requires at least two deformation modes, while validation checks must include an independent mode.

Table 4: Typical calibration/validation matrix.

Data mode	Use in calibration	Use in validation	Notes
Uniaxial tension	Yes	–	Standard ASTM/ISO data
Planar shear	Yes	–	Provides I2 sensitivity
Biaxial inflation	–	Yes	Critical for membranes
Compression	–	Yes	Important for seals

Common Pitfalls

- Using displacement-only elements for incompressible rubbers → volumetric locking.
- Calibrating to uniaxial data only → parameter non-uniqueness.
- Using engineering stress vs true stress inconsistently → 10–30% error.
- Ignoring Mullins effect in cyclic loading → unsafe fatigue predictions.

Conclusion

Accurate FE prediction of elastomeric systems demands appropriate element formulations, robust calibration from multi-mode tests, and rigorous validation against independent data. Engineers must treat model coefficients not as “black box” values but as parameters constrained by test protocols, numerical stability, and physical meaning. When implemented carefully, hyperelastic FE enables predictive design of seals, mounts, and advanced elastomer systems.

Chapter 7: Applications and Case Studies

Introduction

Hyperelastic and advanced elastomer systems find applications across sealing, vibration isolation, biomedical devices, soft robotics, and dielectric actuators. Case studies provide engineers with insight into practical material selection, design, and validation strategies. This chapter presents representative applications, emphasizing lessons learned and pitfalls to avoid. References include Pelrine et al. (2000), Mars and Fatemi (2004), and recent industrial case reports (Roland, 2011; Mark et al., 2013).

Sealing applications

Elastomeric O-rings and gaskets are classic applications. Key requirements are resilience, chemical compatibility, and long-term compression set resistance. For aerospace fuel seals, FKM or FFKM is specified for resistance to jet fuels and hydraulic fluids (Liu and Wu, 2012).

FEA is used to model squeeze and contact pressure distribution, ensuring margins against leakage even after 20–30% compression set.

Vibration isolation mounts

Automotive and machinery mounts use NR or HNBR for dynamic fatigue resistance. FE models must capture shear stiffness and transmissibility at resonance. Case studies show that failing to include Mullins/Payne effects can under-predict damping and lead to cabin noise issues (Mars and Fatemi, 2004).

Biomedical devices

Silicone elastomers dominate medical tubing, catheters, and prosthetics due to biocompatibility and wide service temperature. In heart valve leaflets and artificial muscles, strain to failure and fatigue resistance are critical. Biomechanical FEA must be validated under physiological strain rates and temperatures (Roland, 2011).

Soft robotics and dielectric elastomers

Dielectric elastomer actuators (DEAs) convert electrical to mechanical energy. Prestretched silicone membranes can achieve strains >100% under kilovolt-level fields (Pelrine et al., 2000). FE simulation must couple electrostatics with hyperelasticity. Failure modes include dielectric breakdown and electromechanical instability.

High-temperature sealing in oil and gas

In downhole seals, FKM and FFKM are exposed to >200 °C and aggressive fluids. Case histories show that underestimating swelling and permeation leads to catastrophic blowout preventer failures. Permeation testing per ASTM D471 is critical to verify compound suitability (Liu and Wu, 2012).

Lessons learned

- Always calibrate models to the strain ranges actually encountered.
- Include rate- and temperature-dependent data for applications with cyclic loads.
- Verify sealing stresses after relaxation and aging.
- For new technologies (DEAs, soft robots), build coupled multiphysics FE early to capture instabilities.

Conclusion

Applications demonstrate that elastomer performance depends as much on design and validation as on raw material choice. Case studies in sealing, mounts, biomedical tubing, and DEAs show how hyperelastic FEA combined with fracture/aging considerations can deliver robust performance. Conversely, neglecting Mullins effects, environmental degradation, or multiphysics coupling leads to failures. Engineers must treat elastomer design as a multidisciplinary exercise integrating mechanics, chemistry, and durability science.

Chapter 8: Worked Examples

Introduction

Theory, models, and data protocols are most useful when tied to explicit calculations. The following worked examples illustrate typical design and analysis tasks an engineer may face when using hyperelastic or advanced elastomer systems. They range from simple parameter back-calculations to applied design checks. Each example concludes with an explanation of what the result means in a real-world context.

Example 1: Uniaxial Stress Prediction with the Neo-Hookean Model

Context:

A silicone elastomer for a medical seal is tested in uniaxial extension. The engineering team wants a quick estimate of true stress under a 20% stretch to check whether the material is strong enough to resist assembly loads.

Calculation:

For the incompressible neo-Hookean model:

$$W = \frac{\mu}{2}(I_1 - 3), \qquad \sigma = \mu\,(\lambda^2 - \lambda^{-1})$$

Given μ = 1.0 MPa and λ = 1.20:

$$\sigma = 1.0\,[1.20^2 - (1/1.20)] = 0.607\text{MPa}$$

Result interpretation:

At 20% elongation the elastomer develops ~0.61 MPa true stress. For comparison, the maximum assembly stress is ~0.4 MPa, so the material easily withstands it. However, in-service cyclic loads at higher strains might require validation with more complex models.

Example 2: Calibrating Mooney–Rivlin Constants from Tensile Data

Context:

A nitrile rubber (NBR) fuel hose must be modeled. Engineers have only uniaxial tensile data at two stretch levels due to limited lab resources. They want a quick two-parameter Mooney–Rivlin fit.

Calculation:

Uniaxial nominal stress:

$$P = 2\,(\lambda - \lambda^{-2})\left(C_{10} + \frac{C_{01}}{\lambda}\right)$$

Measured stresses:

$$P(1.20) = 0.70 \text{ MPa},\ P(1.50) = 1.90 \text{ MPa}.$$

Solving simultaneously:

$$C_{10} \approx 1.73 \text{ MPa}, \quad C_{01} \approx -1.25 \text{ MPa}$$

Result interpretation:

The negative C_{01} indicates the model is bending toward an I1-driven response. While this simple calibration reproduces uniaxial data, it must be validated against biaxial or planar tests to avoid unsafe extrapolations.

Example 3: Shear Pad Design for Vibration Isolation

Context:

A machine weighing 50 kg requires vibration isolation at 45 Hz. The engineer specifies a shear-mounted NR pad and needs to confirm natural frequency and transmissibility.

Calculation:

Given: area A = 0.01 m^2, thickness t =20 mm, G =0.8 MPa, damping ratio ζ = 0.08.

- Shear stiffness: $k = GA/\,t$ = 4.0 x 10^5 N/m.
- Natural frequency: $f_n = (1/2\pi)\,\sqrt{k/m} \approx 14.2$ Hz.
- Frequency ratio: $r = f/\,f_n = 45/14.2 \approx 3.16$.

- Transmissibility:

$$T = \sqrt{\frac{1 + (2\zeta r)^2}{(1 - r^2)^2 + (2\zeta r)^2}} \approx 0.124$$

Result interpretation:

Only ~12% of vibration is transmitted, equating to ~18 dB isolation. The pad deflects ~1.2 mm statically, which is acceptable. The design therefore meets both isolation and alignment criteria.

Example 4: Dynamic Properties from DMA

Context:

A designer is selecting an elastomer for a vibration mount and has DMA results at 10 Hz, 23 °C:

E' = 6.0 MPa, tanδ = 0.12. The mount design requires shear modulus inputs.

Calculation:

For incompressible elastomers: $E \approx 3G$.

$$G' = E'/3 = 2.0 \text{ MPa}, \quad E'' = E' \tan\delta = 0.72 \text{ MPa}, \quad G'' = E''/3 = 0.24 \text{ MPa}.$$

Result interpretation:

The material has G = 2.0 + i0.24 MPa. The relatively low damping (tanδ = 0.12) means good stiffness retention but modest energy dissipation. This mount will primarily isolate vibration rather than absorb shocks.

Example 5: Crosslink Density from Shear Modulus

Context:

A silicone compounder wants to estimate network crosslink density to ensure medical tubing will retain flexibility.

Calculation:

For Gaussian networks: $\mu = \nu_e RT$.

Given: μ =1.0 MPa, T =296 K.

$$\nu_e = \frac{\mu}{RT} = \frac{1.0 \times 10^6}{8.314 \times 296} \approx 406 \text{ mol m}^{-3}$$

Result interpretation:

This corresponds to ~0.406 mol L^{-1}. A modest crosslink density ensures flexibility but adequate tensile strength. For higher pressure tubing, a higher density would be desirable, but too much could reduce elongation.

Example 6: Tearing Energy in a Pure Shear Test

Context:

A natural rubber diaphragm must resist crack growth under cyclic flexing. The lab provides strain energy density W = 0.45 MJ/m^3 and specimen half-height h = 5 mm.

Calculation:

For pure shear:

$$T = W \times 2h = 0.45 \times 10^6 \times 0.01 = 4500 \text{ J/m}_2.$$

Result interpretation:

A tearing energy of ~4.5 kJ/m^2 is relatively high, consistent with NR's strain crystallization. The diaphragm is expected to show excellent crack growth resistance compared to SBR or EPDM.

Example 7: Lifetime Prediction by Arrhenius Aging

Context:

EPDM seals in hot water must retain >70% tensile strength after 10 years at 60 °C. Accelerated aging tests show activation energy E_a = 85 kJ/mol. At 100 °C, 50% property loss occurs in 500 hours.

Calculation:

Arrhenius relation:

$$t_1 = t_2 \, exp\left(\frac{E_a}{R}\left(\frac{1}{T_1} - \frac{1}{T_2}\right)\right)$$

With t_2 = 500 h, T_2 = 373 K, T_1 = 333 K:

$$t_1 = 500\ exp\left[\frac{85000}{8.314}(0.003003 - 0.002681)\right] \approx 3.4 \times 10^5 \text{ h}$$

Result interpretation:

Predicted time to 50% strength loss at 60 °C is ~39 years, comfortably exceeding the 10-year design life. The seal design is therefore safe against thermal aging.

Conclusion

Worked examples show how hyperelastic models, fracture mechanics, and viscoelastic theory translate into practical engineering insights: verifying stress levels, fitting parameters, designing isolation systems, assessing dynamic properties, evaluating durability, and predicting lifetime. Contextual interpretation is as critical as the calculation itself: without clear understanding, numerical values risk being misapplied. For professional engineers, these examples illustrate the bridge between laboratory data, constitutive modeling, and safe, durable elastomeric designs.

Bibliography

1. Abaqus (2024) *Hyperelastic material behavior; Compressibility; Hybrid elements recommendations*. Dassault Systèmes documentation (accessed 2025).
2. ANSI/ASTM (various years) *ASTM D412—Vulcanized Rubber and Thermoplastic Elastomers—Tension*; *ASTM D2240—Durometer Hardness*; *ASTM D395—Compression Set*; *ASTM D471—Rubber Property—Effect of Liquids*; *ASTM D5289—Vulcanization Using Rotorless Cure Meters*. West Conshohocken, PA: ASTM International.
3. Arruda, E.M. and Boyce, M.C. (1993) A three-dimensional constitutive model for the large stretch behavior of rubber elastic materials. *Journal of the Mechanics and Physics of Solids*, 41(2), pp. 389–412.
4. Belytschko, T., Liu, W\.K. and Moran, B. (2014) *Nonlinear Finite Elements for Continua and Structures*. 2nd edn. Wiley.
5. Bergström, J.S. and Boyce, M.C. (1999) Mechanical behavior of particle filled elastomers. *Rubber Chemistry and Technology*, 72(4), pp. 633–656.
6. Crack, C.J., et al. (2010) Ozone resistance of elastomeric seals in automotive environments. *Polymer Degradation and Stability*, 95(12), pp. 2474–2480.
7. Diani, J., Fayolle, B. and Gilormini, P. (2009) A review on the Mullins effect. *Polymer Testing*, 29(2), pp. 199–209.
8. Elmukashfi, E., Kroon, M. and Trygg, J. (2021) An experimental method for estimating the tearing energy in rubber-like materials using the true stored energy. *Scientific Reports*, 11, 16016.
9. Ferry, J.D. (1980) *Viscoelastic Properties of Polymers*. 3rd edn. New York: Wiley.
10. Gent, A.N. (1996) A new constitutive relation for rubber. *Rubber Chemistry and Technology*, 69(1), pp. 59–61.
11. Holzapfel, G.A. (2000) *Nonlinear Solid Mechanics: A Continuum Approach for Engineering*. Wiley.
12. Holden, G., Kricheldorf, H.R. and Quirk, R.P. (eds.) (2004) *Thermoplastic Elastomers*. 3rd edn. Hanser.
13. ISO (2017–2024) *ISO 37—Rubber, vulcanized or thermoplastic—Determination of tensile stress–strain properties*; *ISO 815-1—Determination of compression set*; *ISO 4666—Rubber, vulcanized or thermoplastic—Determination of dynamic properties in flexometer testing*. Geneva: International Organization for Standardization.
14. Lake, G.J. and Thomas, A.G. (1967) The strength of highly elastic materials. *Proceedings of the Royal Society A: Mathematical, Physical and Engineering Sciences*, 300(1460), pp. 108–119.

15. Liu, J. and Wu, S. (2012) High-temperature performance of fluoroelastomers. *Journal of Applied Polymer Science*, 124(1), pp. 49–58.
16. Mark, J.E., Erman, B. and Roland, C.M. (2013) *The Science and Technology of Rubber*. 4th edn. Academic Press.
17. Mars, W\.V. and Fatemi, A. (2004) A literature survey on fatigue analysis approaches for rubber. *International Journal of Fatigue*, 26(9), pp. 949–963.
18. Mooney, M. (1940) A theory of large elastic deformation. *Journal of Applied Physics*, 11(9), pp. 582–592.
19. Ogden, R.W. (1997) *Non-Linear Elastic Deformations*. New York: Dover.
20. Pelrine, R., Kornbluh, R. and Kofod, G. (2000) High-speed electrically actuated elastomers with strain greater than 100%. *Science*, 287(5454), pp. 836–839.
21. Qi, H.J. and Boyce, M.C. (2004) Constitutive model for stretch-induced softening of the stress–strain curve of elastomeric materials. *Journal of the Mechanics and Physics of Solids*, 52(10), pp. 2187–2205.
22. Rivlin, R.S. (1948) Large elastic deformations of isotropic materials. *Philosophical Transactions of the Royal Society A*, 240(822), pp. 459–490.
23. Rivlin, R.S. and Thomas, A.G. (1953) Rupture of rubber. I. Characteristic energy for tearing. *Journal of Polymer Science*, 10(3), pp. 291–318.
24. Roland, C.M. (2011) *Viscoelastic Behavior of Rubbers*. Oxford: Oxford University Press.
25. Ward, I.M. and Sweeney, J. (2013) *Mechanical Properties of Solid Polymers*. 3rd edn. Wiley.
26. Williams, M.L., Landel, R.F. and Ferry, J.D. (1955) The temperature dependence of relaxation mechanisms in amorphous polymers and other glass-forming liquids. *Journal of the American Chemical Society*, 77(14), pp. 3701–3707.
27. Figure 1: Bbanerje, CC BY-SA 3.0 <https://creativecommons.org/licenses/by-sa/3.0>, via Wikimedia Commons

Educational Use Only

The content of this course is provided for educational purposes only. While every effort has been made to ensure the accuracy and reliability of the information presented, the author or publisher makes no guarantees regarding the completeness or applicability of the information to specific professional practices. Users are advised to consult additional resources and exercise professional judgment when applying the knowledge contained in this course.

Use of AI Generated Content

The continuing education (CE) courses offered on this platform are developed using advanced artificial intelligence (AI) methodologies to generate high-quality, text-based instructional content.

These courses are primarily designed to provide in-depth knowledge on engineering and technical subjects with minimal or no imagery, focusing on comprehensive textual explanations to convey concepts effectively.

While every effort is made to ensure accuracy, clarity, and compliance with professional standards, the nature of AI-assisted content generation means that occasional errors or inconsistencies may occur. Users are encouraged to critically evaluate the material and verify key technical details as needed. Additionally, these courses do not include interactive elements or extensive visual aids such as diagrams, charts, or illustrations unless explicitly stated.

By enrolling in and using these courses, participants acknowledge and accept that the content is primarily text-based and generated through AI-assisted processes. The course provider assumes no liability for any inaccuracies or omissions and advises professionals to apply their own judgment and expertise when utilizing course materials in practical applications.